Diffusion enhancement and autoparametric resonance

Johann Maddi, Christophe Coste, and Michel Saint Jean
Laboratoire "Matière et Systèmes Complexes" (MSC), UMR 7057 CNRS, Université Paris–Diderot (Paris 7), 75205 Paris Cedex 13, France

(Received 22 January 2024; accepted 10 April 2024; published 6 May 2024)

The possibility of an autoparametric resonance in an isolated many-particle system induces a specific behavior of the particles in the presence of thermal noise. In particular, the variance associated with a resonant mode, and consequently that of the associated particles, is strongly increased compared to what it would have in the absence of parametric resonance. In this paper we consider a dimer submitted to a periodic potential for which there are only two modes, the center of mass motion and the internal vibration mode. This is the simplest system which is dynamically rich enough to exhibit an autoparametric excitation of the internal vibrations by the center of mass motion. The consequences of this autoparametric excitation on the particles diffusion will be discussed according to the stiffness of the interaction and to the initial energy of the dimer, the relevant parameters which characterize this dynamics.

DOI: 10.1103/PhysRevE.109.054107

I. INTRODUCTION

How can the thermal diffusion of a system be enhanced by an underlying periodic potential? The answer to this question is not obvious since all the studies concerning the diffusion of a single particle in a periodic potential (for a review, see chapter 11 in [1]), whether symmetrical [2–4] or not [5,6], static [7,8], pulsating [9], or fluctuating [10], exhibit in contrast a slowing down of its diffusion. Indeed, crossing the energy barriers E_B associated with the periodic potential results in a smaller diffusion coefficient D than the free diffusion coefficient D_0. The activated diffusion coefficient reads $D = D_0 e^{-E_B/k_B T}$ (Kramer Relation) where $D_0 = k_B T/2m\gamma$ (m the particle mass, γ the damping coefficient, and T the thermodynamic temperature) [11,12]. However, this diffusion can be increased by applying a force and becomes maximum when this force reaches a depinning threshold, which allows one to overcome the potential barriers [13].

The diffusion of a system of interacting particles is somewhat different. Let us consider a chain of interacting particles confined along a straight line in such a way that they cannot cross each other. Without any periodic longitudinal (that is, along the direction of the chain) potential, the thermal motions of the chain are described by the Single File Diffusion (SFD) theory. The particles transport is strongly subdiffusive, with a mean square displacement of the particle position that scales as $t^{1/2}$ [14–19]. In the presence of an underlying potential, various mechanisms resulting in an increasing of this transport have been identified according to the physical situations encountered. The focus is then put on the role played by the commensurability between the period of the system and that of the potential on the increase of this mobility. Another mechanism invoking a transfer of fluctuations from an incommensurable and fluctuating over time potential to a chain of interacting particles has been more recently suggested to explain the enhancement of their thermal diffusion [20]. A similar enhancement has been observed in an asymmetric potential such that the curvature at the maxima is smaller than the curvature at the minima, with a spatial period of the potential that is twice the distance between particles [21].

Other studies devoted to the diffusion of a system of two particles in elastic interaction on a periodic potential, either with [22–24] of without [25] a constant applied force, are the first to mention the importance of the dynamics of the center of mass on the relative motion, because of the nonlinear coupling induced by the underlying potential. This physical effect, early mentioned to explain the strong dependence of the desorption mechanisms of long molecules with their transverse modes of vibration [26], was used to analyze the peaks observed in the variations of the diffusion coefficient $D(F)$ with the applied force F and their dependence with the dimer stiffness. While for a rigid (weakly deformed) dimer in a potential $D(F)$ has a unique peak when the force F is close to the depinning threshold [24,27–30], the dynamics of the center of mass becomes more complex when the stiffness of the dimer decreases. The evolution of $D(F)$ as a function of the force F and the relevant interpretation differ from one study to another. For instance, the simulations of Braun *et al.* [23] showed that $D(F)$ has one peak for an incommensurable system and two for a commensurable one. According to these authors, these two peaks result from the commensurability of the system with the potential. The studies carried out by Heinsalu *et al.* [24] give a different result. According to the stiffness K and the damping coefficient γ, the variation of $D(F)$ may present one or two peaks in the commensurable case, but two peaks may also be observed with incommensurable systems. For these authors, the number of peaks results from the ratio between elastic and dissipated energies.

The origin of the single peak or of the one associated with the weakest force when two peaks are observed is consensually attributed to a depinning effect. In order to interpret the appearance of a second peak, Braun *et al.* suggested, without much precision, that the second peak could be due to the coupling between the center of mass motion and the dimer internal vibration [23]. This idea was then deepened by

Heinsalu *et al.*, who considered that the second peak was due to the parametric resonance of the internal vibration induced by the center of mass motion and to the applied force [24]. According to them, the second peak would appear for the applied force such that the induced translation speed would correspond to a forcing frequency that would match the internal vibration frequency. Among the arguments put forward to validate this hypothesis, the authors suggested the sensitivity of peaks to variations of the dimer stiffness K and the dissipation γ. Indeed, if the dimer is too soft, the two peaks merge and the diffusion becomes that of the almost free particles constituting the dimer. Similarly, if the dissipation is large enough to annihilate the parametric resonance, the second peak vanishes. Moreover, this mechanism would be totally independent of the commensurability of the system. So, while the existence of this second particular force is clearly explained, the fact that it induces an increase in the center of mass diffusion is not detailed. Note, finally, that a few years earlier, studies in the absence of applied force of the diffusion of the center of mass of a dimer according to its length and stiffness had shown that an Arrhenius law was followed only in the commensurable case, this diffusion being even greater than that of a particle in the incommensurable case [29,31]. This discrepancy of results and of analyses results probably because of the large number of parameters controlling the parametric resonance and thus the dimer diffusion.

This article focus on the specific influence of the parametric resonance of vibration modes on the diffusion of the dimer. In order to deal with all possible dynamic situations, including those where the mass center of the dimer is trapped in a potential well, we use the word "diffusion" in a very broad sense. When the dimer is trapped, the fluctuations of position remain bounded at all times, our observable is the variance of these fluctuations, and it is in this sense that we study the diffusion of the dimer.

To get rid of the effects of commensurability and tilt, our simulations have been performed for a dimer whose length is equal to the period of the static potential and without any constant applied force. In a first part we shall quickly recall the known results concerning the parametric resonance of such a dimer [32,33]. Particular emphasis will be placed on the precise identification of the stiffness values and the initial energy of the system for which the dimer is in its instability domain. The cases of a dimer "trapped" in the wells of potential and that of a "sliding dimer" moving over the periodic potential will be successively considered. In a second part the results obtained concerning the diffusion of the center of mass and the relative motion mode in the parametric resonance regime previously identified will be presented. We will point out that parametric resonance greatly amplifies the relative motion diffusion and discuss the dependence of these fluctuations increasing according to the initial energy E_0 of the dimer and to the stiffness K.

II. AUTOPARAMETRIC RESONANCE OF A DIMER

We study a system of two identical interacting particles of mass m that move along the x axis. They are located at positions x_1 and x_2, and their interaction is modeled by a linear spring of stiffness k and equilibrium length d. In the presence of an underlying commensurate sinusoidal potential $U(x_1, x_2)$ of period d, the equations of motions are

$$m\ddot{x}_1 = k(x_2 - x_1 - d) - (2\pi U_0/d)\sin(2\pi x_1/d), \quad (1)$$

$$m\ddot{x}_2 = k(x_1 - x_2 + d) - (2\pi U_0/d)\sin(2\pi x_2/d), \quad (2)$$

where $\ddot{x}_i \equiv \mathrm{d}^2 x_i/\mathrm{d}t^2$.

We rescale the variables using $d/2\pi$ as the unit length and U_0 as the unit energy, so that $\sqrt{md^2/4\pi^2 U_0}$ is the unit time. We introduce the normal modes as

$$x \equiv \frac{x_1 + x_2}{2} - \pi, \quad y \equiv \frac{x_2 - x_1}{2} - \pi \quad (3)$$

in dimensionless units, where x is the center of mass (CM) coordinate and y is the relative motion (RM). With these variables, the equations of motion become

$$\ddot{x} = -\sin x \cos y, \quad (4)$$

$$\ddot{y} = -2Ky - \cos x \sin y, \quad (5)$$

where $K = kd^2/4\pi^2 U_0$ is the dimensionless stiffness. Here the underlying potential is

$$U(x, y) = 2(1 - \cos x \cos y), \quad (6)$$

so that it induces a nonlinear coupling between the eigenmodes. It is this coupling which induces the parametric resonance of the system.

Three main dynamic regimes of the dimer may be identified according to the initial energy E_0 of the system [33]. When $E_0 < 4$, the dimer is *trapped*, the CM motion $x(t)$ and the RM $y(t)$ oscillate in their respective (effective) well. When $E_0 > 4$, the CM trajectory may extend over several potential energy wells. When the CM trajectory evolves monotonously with time, we will speak of a *sliding regime*. The third dynamical regime will be called the *jumping regime*. In a trapped configuration, it corresponds to large enough deformations of the dimer for the particles to oscillate in nonadjacent potential wells. In a sliding configuration, the CM trajectory ceases to be monotonous and alternates between oscillations and translations over more than one spatial period of the underlying potential. Whatever the considered regime, it was shown that the RM may be parametrically excited by the oscillations of the CM in the case of a trapped dimer or by its translation in the case of the sliding dimer [29,32]. In contrast, the CM cannot be excited by the oscillations of the RM [32]. So in the following we shall focus on the conditions of the RM parametric resonance. This resonance is said to be *autoparametric* since no external operator acts upon the system.

In order to determine the domain in the parameter space (K, E_0) of parametrically unstable RM, the linear stability analysis is sufficient [29,32]. Therefore we assume $|y(t)| \ll 1$ so that Eqs. (4) and (5) now read

$$\ddot{x} = -\sin x, \quad (7)$$

$$\ddot{y} = -2Ky - y\cos x. \quad (8)$$

When the dimer is trapped ($E_0 < 4$), the CM motion is very well described by $x(t) = a\sin\omega_x t$ where $\omega_x = 1 - a^2/16$ is the Borda frequency. Injecting this expression in the RM

equation, we obtain

$$\ddot{y} = -\left(\omega_y^2 + \frac{a^2}{4}\cos 2\omega_x t\right)y, \quad \omega_y^2 \equiv 2K + \left(1 + \frac{a^2}{4}\right). \quad (9)$$

We recognize a Mathieu equation, which describes the dynamics of an oscillator whose natural frequency is modulated with time [34,35]. This oscillator reaches its instability domain as soon as the frequency ω_y is close to the frequency ω_x. Note that this condition implies a small enough stiffness. The extent of the instability domain depends upon the forcing amplitude [34]. The instability condition is given by

$$a^2/8 > \left|\omega_y^2 - \omega_x^2\right| \quad \Longrightarrow \quad E_0/8 \equiv K_I > K. \quad (10)$$

The last inequality comes from the fact that at lowest order in the CM amplitude a we have $E_0 = a^2$ [32].

When $E_0 > 4$, the trajectory of the CM of a dimer in its "sliding regime" is basically a straight line. When E_0 is close to 4, this trajectory is modulated since the CM motion becomes sensitive to the underlying potential, but we have shown that this modulation has only a small influence on the limits of instability domain [32]. So the CM trajectory $x(t)$ is well approximated by $x(t) = V_M t$ where $V_M = E_0^{1/2}(1 - 1/E_0)$ is the mean velocity of the CM [29,32], which takes into account the mean energy shift 2 induced by the underlying potential. Proceeding as before, the equation of motion of the RM now reads

$$\ddot{y} = (2K + \cos V_M t)y. \quad (11)$$

The condition of instability is now given by

$$1/2 > |2K - (V_M/2)^2| \quad \Longrightarrow \quad E_0/8 > K > (E_0 - 4)/8. \quad (12)$$

In what follows we define $K_I^> \equiv E_0/8$ and $K_I^< \equiv (E_0 - 4)/8$. Both boundaries in the parameter space (K, E_0) are straight lines, and the lower boundary extends the straight line (10) found in the trapped case.

The calculated boundaries of the parametric instability domain have been compared with numerical simulations of the full nonlinear system of Eqs. (4) and (5). In Fig. 1 we classify the behaviors of the dimer in the parameter plane (E_0, K). This map extends that of Ref. [33] and include results from 8.5×10^5 simulations. The calculated boundaries (10) and (12) are plotted as thick straight lines, and they match perfectly with the simulation data.

III. TRANSIENT ENHANCEMENT OF DIFFUSION

In order to take into account the effect of a thermal bath on the dimer, we introduce a dissipation coefficient γ and statistically independent Gaussian random forces $\mu_1(t)$ and $\mu_2(t)$ on the particles, so that the equations of motions for the modes (4) and (5) now become

$$\ddot{x} = -\sin x \cos y - \gamma\dot{x} + \mu_x(t), \quad (13)$$

$$\ddot{y} = -2Ky - \cos x \sin y - \gamma\dot{y} + \mu_y(t), \quad (14)$$

where we define $\mu_x(t) \equiv [\mu_1(t) + \mu_2(t)]/2$ and $\mu_y(t) \equiv [\mu_2(t) - \mu_1(t)]/2$. These random forces are such that

$$\langle \mu_i(t) \rangle = 0, \quad \langle \mu_i(t)\mu_j(t') \rangle = 2\Theta\gamma\delta_{ij}\delta(t - t'), \quad (15)$$

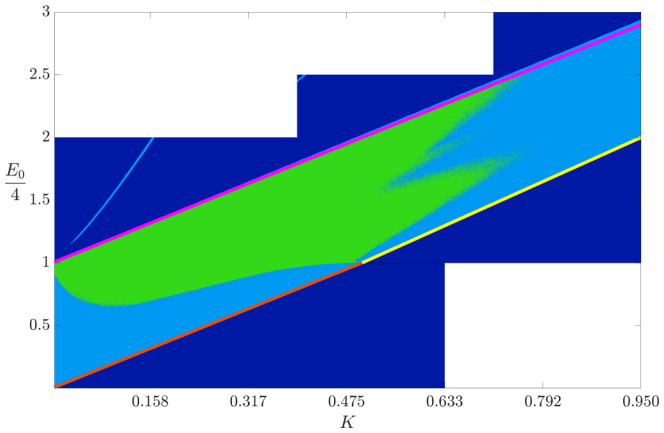

FIG. 1. Dimer behavior map in the parameter space (K, E_0) where K is the stiffness of the harmonic interaction and E_0 the initial energy of the dimer, injected in the CM motion. The initial energy of the RM is $10^{-3}E_0$. The dark blue (dark gray) areas represent a parametrically stable RM. The light blue (light gray) areas represent a parametrically unstable RM. The green area (medium gray) represents jumping motions of the system. The orange line is the instability threshold K_I, the yellow line is the instability threshold $K_I^<$, and the upper magenta line is the instability threshold $K_I^>$.

where the index $i \in \{x, y\}$ and where $\langle\cdot\rangle$ means statistical average. In our dimensionless units $\Theta = k_B T/U_0$ where k_B is Boltzmann constant and T the thermodynamic temperature, and γ is the dimensionless dissipation coefficient built with the unit time.

The system of coupled nonlinear Langevin equations (13) and (14) is then numerically integrated [36,37]. The relevant observables are the variances of the position of the CM $\sigma^2(x)$ and of the relative motion amplitude $\sigma^2(y)$. These variances are function of the time t, but we do not indicate this dependency for the sake of brevity. In this section we focus on their evolution with time when the initial energy E_0 of the dimer and the stiffness K of the harmonic interaction vary. The statistical averages are made on 150 simulations for each pair of parameters (K, E_0) considered. All simulations were carried out in the underdamped regime ($\gamma \ll 1$), since high dissipation suppresses the effect we want to highlight.

Because of the dissipation the energy of the dimer is not conserved and the representative point in the map of Fig. 1 follows a trajectory of decreasing energy at constant stiffness K. Therefore, whatever its initial energy E_0 the dimer eventually reaches at long times its thermodynamic equilibrium in a trapped state. We will return to the subject in more detail in Sec. III B 2.

It should also be stressed that when the energy of the system is below 4, the diffusion of the dimer is sensitive to the anharmonicity of the underlying potential. As an example, we plot in Fig. 2 the variances of a particle trapped in the potential $(x^2 - x^4/12)$ [the expansion of (6) up to x^4 for vanishingly small y] for several values of its initial energy and compare it to the variance of the same particle in the same conditions but in a quadratic potential x^2. It is important to remark that the variance in a quartic potential strongly depends upon the initial energy of the particle in contrast with the case of the quadratic potential. Moreover, between the initial ballistic

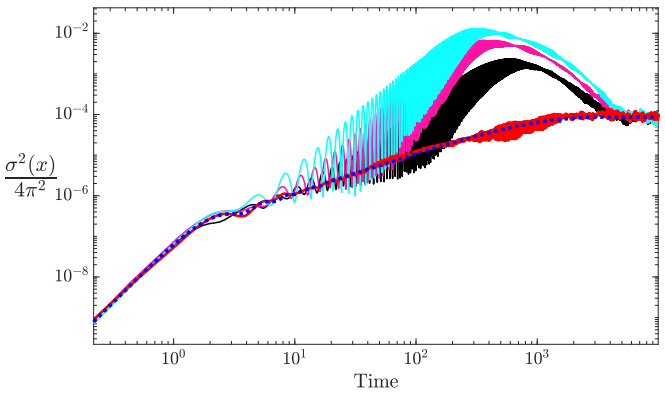

FIG. 2. Variance $\sigma^2(x)$ of a single particle as a function of time, in dimensionless units, in the potential $(x^2 - x^4/12)$. The dissipation is $\gamma = 1.3 \times 10^{-3}$, and the thermal energy is $\Theta = 7.0 \times 10^{-3}$. The dashed blue line is the variance of the particle in an harmonic potential. The initial energy E_0 of the particle is 0.02 (red, dark gray), 0.40 (black), 0.92 (magenta, medium gray), and 1.40 (cyan, very light gray).

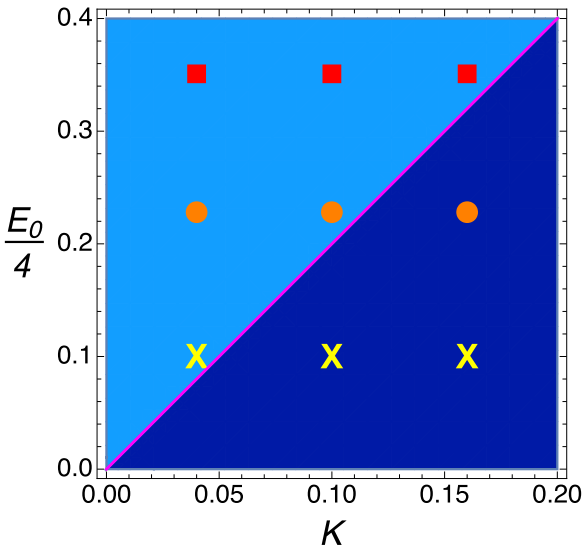

FIG. 3. Representative points for the initial energy E_0 and the stiffness K_i in the parameter space for the simulations described in Fig. 4. The stiffnesses are indexed in increasing order, with $K_1 = 0.04$, $K_2 = 0.10$, and $K_3 = 0.16$. The initial energies are $E_0 = 0.40$ (yellow, very light gray, crosses), $E_0 = 0.92$ (orange, medium gray, disks), and $E_0 = 1.40$ (red, dark gray, filled squares).

regime and the eventual equilibrium regime, the variance in the quartic potential is significantly higher than in the harmonic potential. This transient growth of fluctuations is all the greater and appears all the earlier as the initial energy is higher. As we shall see, this behavior differs significantly from that implied by the parametric resonance of the dimer when it is initially in the sliding regime ($E_0 > 4$). This transitory amplification of the variance decreases with damping. Note also that the variance $\sigma^2(y)$ exhibits the same characteristics; in particular the earliest growth is associated with the system of higher initial energy.

A. Transient enhancement of a trapped dimer diffusion

A dimer is initially trapped if $E_0 < 4$. As seen in Fig. 1, for sufficiently low stiffness and high enough initial energy the system may be in a jump configuration. In this section we do not consider this case and defer its discussion in Sec. III C. To be specific, we consider the simulations that have been performed for nine different initial configurations indicated on the behavior map in Fig. 3. In order to facilitate the reading, from now on the stiffness will be numbered in ascending order, and the initial energies will go in ascending order from yellow crosses, orange disks, and red squares. The plots of the variances $\sigma^2(x)$ and $\sigma^2(y)$ are shown in Fig. 4 as a function of time, with the same color code as the relevant initial energy used in the simulations.

When the initial conditions are in the stable area, the initial energy is high enough for the variance $\sigma^2(x)$ to be similar to that of a single particle in an anharmonic well, as evidenced by the comparison between Fig. 2 and the relevant plots in Fig. 4 (K_2, yellow solid line and K_3, yellow and orange solid lines). The long time limit for $\sigma^2(x)$ is found to be $\Theta/2$ [the unusual factor 2 results from the definition of the CM in Eq. (3)], and the variances depend only slightly on stiffness. For the RM, the variance $\sigma^2(y)$ is very close to that of an harmonic oscillator diffusing in an harmonic potential well, as evidenced by the comparison of the relevant plots with the dotted cyan plot. Consistently, the long time limit for $\sigma^2(x)$ is found to be $\Theta/2(2K + 1)$ whatever the initial energy E_0. These plots will serve as a reference for identifying specific effects due to the parametric resonance on the RM variance.

The observed behaviors are very different when the initial configuration of the dimer is such that the RM is parametrically unstable. Indeed, let's look at the variances $\sigma^2(y)$ for the three red systems, which all have an initial energy above the instability limit. All of them exhibit a transient behavior (roughly on three orders of magnitude in time) with a variance that is much higher (up to two orders of magnitude at the maximum) than the variance of a trapped oscillator with the same stiffness, but without the parametric resonance. In this transient, oscillations are seen that correspond to the slow modulation of the RM amplitude induced by the autoparametric resonance. This variance then decreases exponentially. Because of the dissipation, eventually the system exits the parametric instability zone, and its variance reaches the asymptotic value $\Theta/2(2K + 1)$ for a thermal energy Θ. Schematically the time evolution of $\sigma^2(y)$ may be described by four successive sequences: a ballistic regime, a rapid increase due to RP followed by a decrease due to damping, and nally a thermodynamic equilibrium regime at a long time.

More precisely, the greater the part of the instability area crossed, the greater the increase in the RM variance. Indeed, as seen from the representative points of the initial conditions in Fig. 3, when the stiffness decreases from K_3 to K_1 while the initial energy is constant, the distance (in the parameter plane) to the instability limit increases. Since the dissipation is the same for all simulations in Fig. 4 the time spent by the system in the unstable zone certainly increases with decreasing

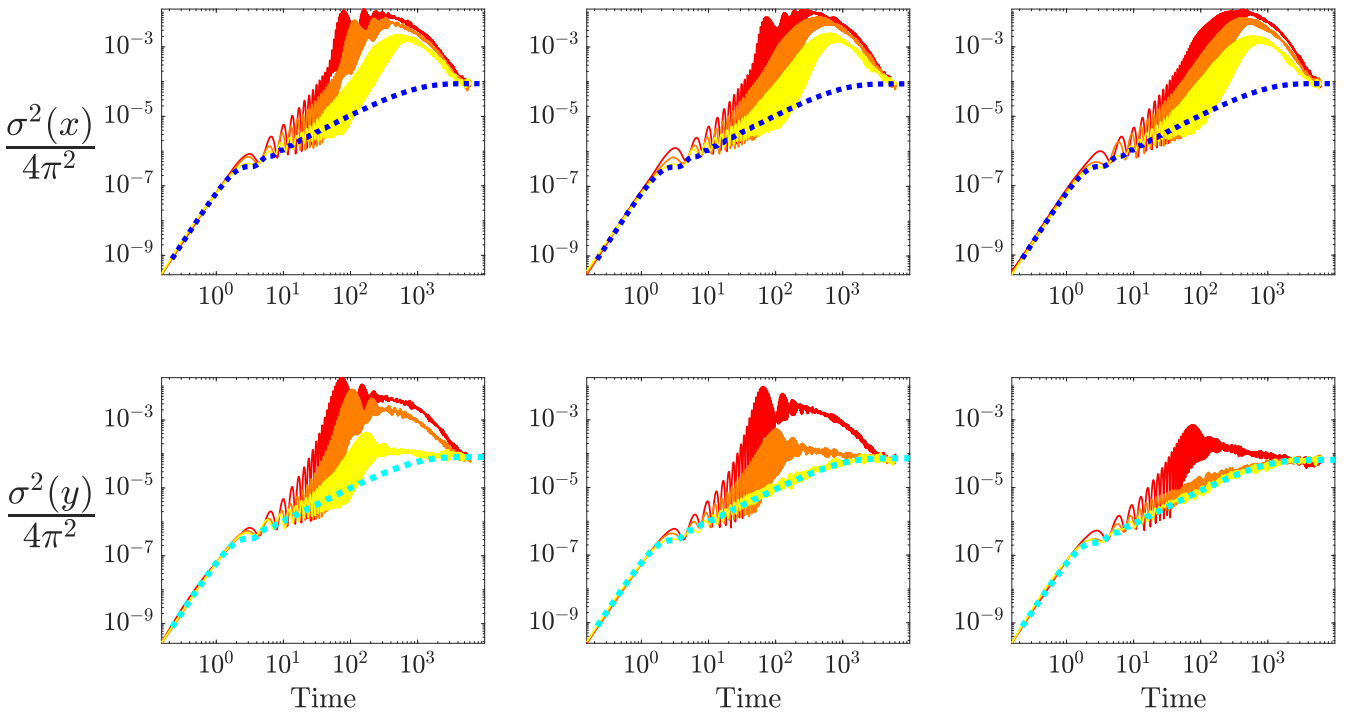

FIG. 4. Plots of the variances $\sigma^2(x)$ (top plots) and $\sigma^2(y)$ (bottom plots) as a function of time t for the initial conditions of Fig. 3, and for $\Theta = 7.0 \times 10^{-3}$ and $\gamma = 1.3 \times 10^{-3}$. The stiffnesses increase from left to right. The blue (resp. cyan) dashed lines correspond to the diffusion of a single particle in an harmonic well of frequency 1 (resp. $\sqrt{2K+1}$).

stiffness. For a given initial energy, the maximum of the RM variance decreases with the dimer stiffness (consider the red plots). In the same fashion, the variances $\sigma^2(y)$ for the systems with stiffness K_1, which are all initially parametrically unstable, all exhibit an enhanced transient whose maximum value is the greater the higher the initial energy compared to the instability boundary. These observations evidence that the variance enhancement is a cumulative effect, which is a first characteristic of the parametric instability [32]. A second characteristic of the parametric resonance of a trapped system is that the increase in the RM variance appears all the earlier the initial energy is large.

The effect of parametric resonance on the CM variance $\sigma^2(x)$ is smaller but observable. We have seen that when the system is initially in the stable area, this variance is basically that of an effective particle trapped in an anharmonic potential. In contrast, the variance for systems that are parametrically unstable such as those with stiffness K_1 and initial energy corresponding to the orange and red dots in Fig. 3 exhibit qualitative differences with the variance of a particle in an anharmonic well. This is seen in Fig. 5. The yellow plot corresponds to a low-energy dimer that is parametrically stable, and its variance is found to be roughly the same as that of a particle in an anharmonic well. For the other higher initial energies (orange then red plots) the dimer is parametrically unstable, and its variance exhibits modulations that make it clearly different from the variance of a particle in an anharmonic well. The link with the parametric resonance is all the more clear since these modulations are synchronous with the beginning of amplification of the RM variance.

When the damping increases, these effects gradually disappear. Two physical mechanisms can be invoked. Greater dissipation implies a faster decrease in energy, and therefore all else equal to a shorter stay in the parametrically unstable zone of the behavior map. This reduces all the more the influence of parametric resonance, which we have seen was a cumulative phenomenon. Moreover, a parametric forced oscillator is less unstable because it is more dissipative, with constant parametric forcing. Figures 6 and 7, which are respectively obtained for a dissipation that is ten times higher

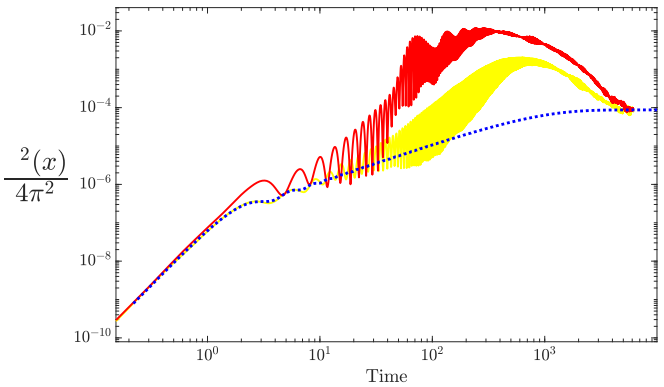

FIG. 5. Variances $\sigma^2(x)$ as a function of time, in dimensionless units. The dissipation is $\gamma = 1.3 \times 10^{-3}$, the thermal energy is $\Theta = 7.0 \times 10^{-3}$, and the dimer stiffness is $K_2 = 0.1$. The dashed blue line is the variance of the particle in an harmonic potential. Yellow (light gray) solid line, parametrically stable dimer ($E_0 = 0.40$). Red (dark gray) solid line, parametrically unstable dimer ($E_0 = 1.40$).

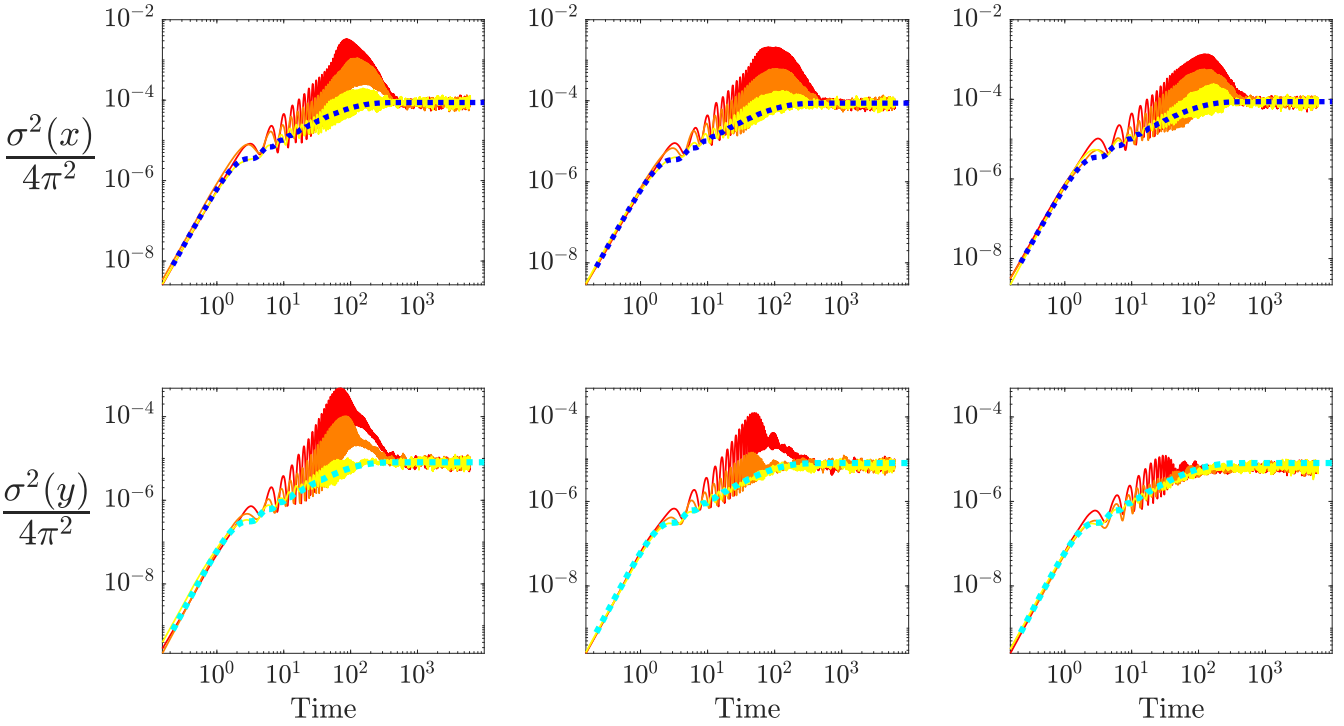

FIG. 6. Same as Fig. 4, but for a dissipation $\gamma = 1.3 \times 10^{-2}$.

and 100 times higher than that of Fig. 4, give evidence of such behavior.

B. Transient enhancement of a sliding dimer diffusion

An initially sliding dimer has an initial energy $E_0 > 4$. Because of the dissipation, the sliding velocity of the CM decreases, hence its kinetic energy, until the dimer becomes trapped. In Sec. III B 1 we estimate in a simple fashion the relevant timescales for this energy decrease. The dimer diffusion exhibits peculiar effects if, for a given stiffness K of the interaction, the dimer energy enters the parametrically unstable strip in the behavior map (see Fig. 1). In Sec. III B 2 we

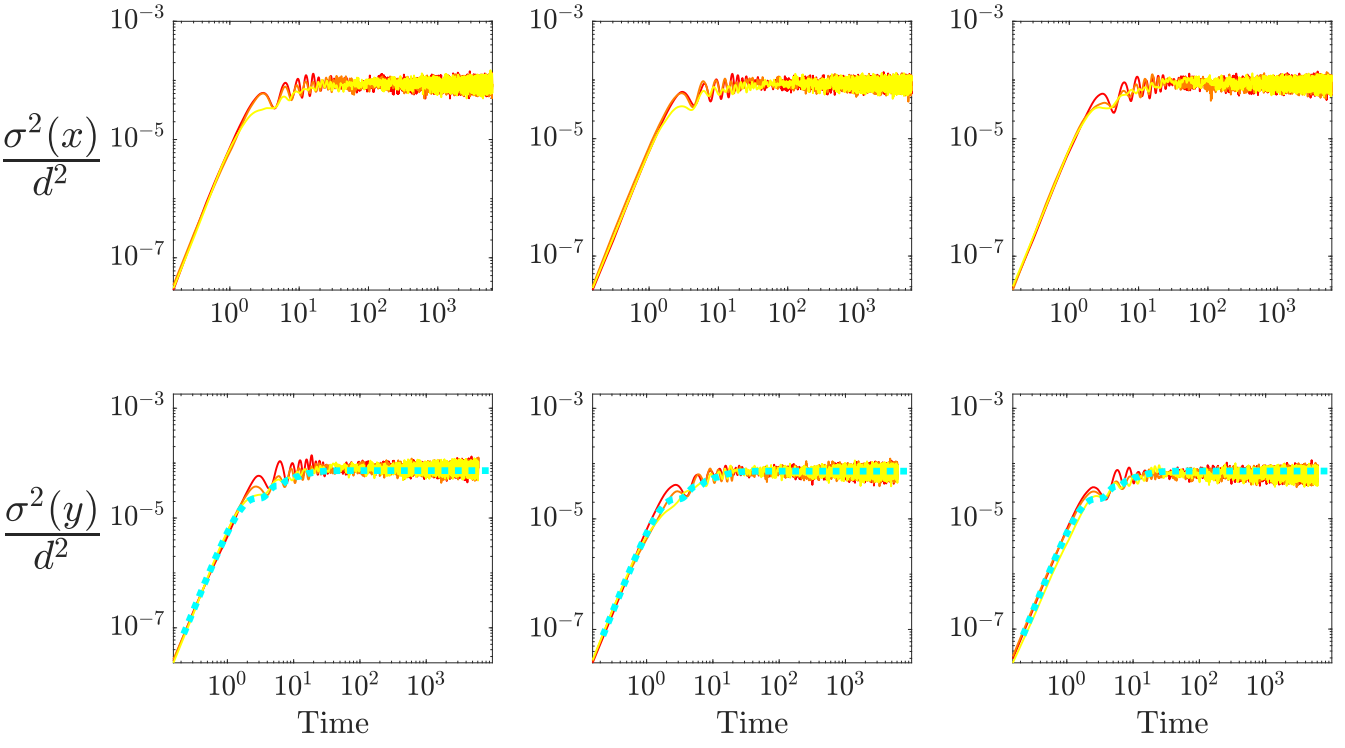

FIG. 7. Same as Fig. 4, but for a dissipation $\gamma = 1.3 \times 10^{-1}$.

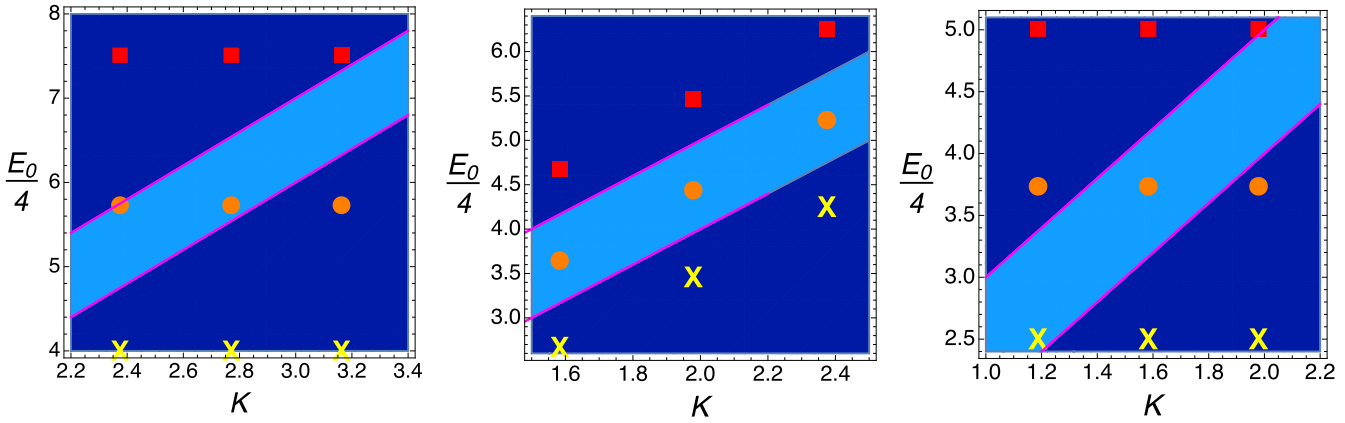

FIG. 8. Three sets of initial conditions in the parameter plane (K, E_0) such that the corresponding systems never reach a jump configuration when their energy decreases due to dissipation. The dark blue areas represent a parametrically stable RM. The light blue areas represent a parametrically unstable RM. The corresponding variances are plotted in Fig. 9 for the leftmost set, in Fig. 10 for the center set, and in Fig. 11 for the rightmost set. The relevant numerical values of the stiffness K and the initial energy E_0 are given in the captions.

document the behavior of those systems that are stiff enough not to enter in a jumping regime when the RM becomes parametrically unstable. The behavior of systems with a jump regime is discussed in Sec. III C for systems that are initially sliding and for systems with low enough stiffness to be in a jump regime with an initial energy below 4.

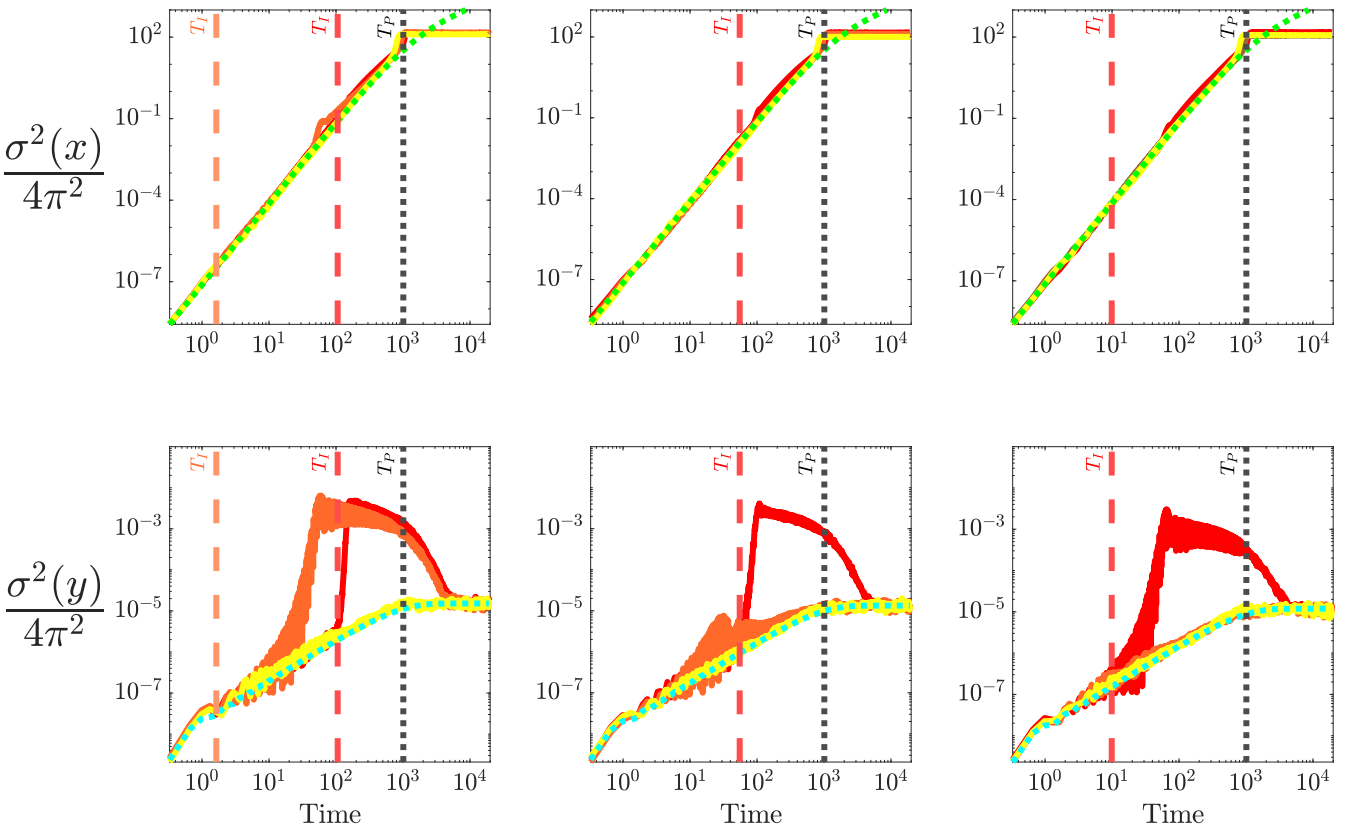

FIG. 9. Plots of the variances $\sigma^2(x)$ (top plots) and $\sigma^2(y)$ (bottom plots) as a function of time, in logarithmic scales, for the initial conditions displayed in the leftmost map of Fig. 8, for $\Theta = 7.0 \times 10^{-3}$ and $\gamma = 1.3 \times 10^{-3}$. The stiffnesses are $K_1 = 2.3747$, $K_2 = 2.7705$, and $K_3 = 3.163$. The initial energies are $E_0 = 16$ (yellow, light gray, solid line), $E_0 = 23$ (orange, medium gray, solid line), and $E_0 = 30$ (red, dark gray, solid line). The green dashed lines correspond to the diffusion of a single free particle; the cyan dashed lines to the diffusion of a single particle in an harmonic well of frequency $\sqrt{2K+1}$. The times T_I of Eq. (21) are indicated by dashed lines of the same color as the relevant plot, the time T_P by a black dotted line.

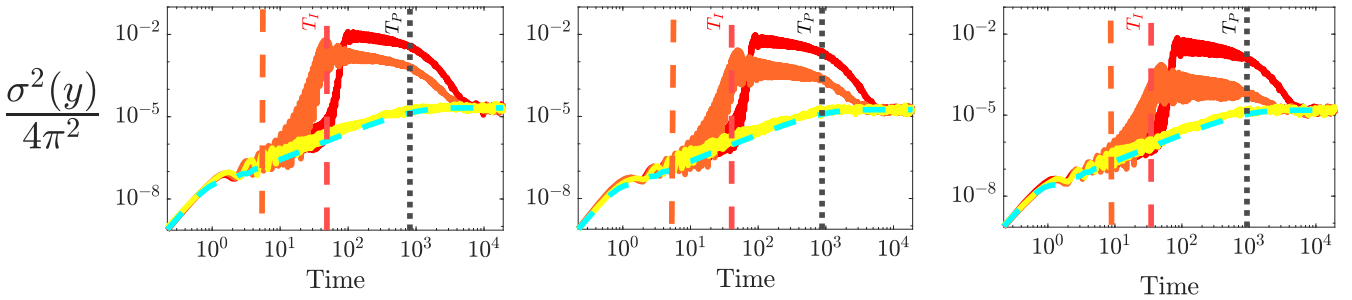

FIG. 10. Plots of the variances $\sigma^2(y)$ as a function of time, in logarithmic scales, for the initial conditions displayed in the center map of Fig. 8. The stiffnesses are $K_1 = 1.5831$, $K_2 = 1.9789$, and $K_3 = 2.3747$. For a given stiffness, the energies increase in order yellow (light gray), orange (medium gray), then red (dark gray). The initial energies are $E_0 = 32/3$, $E_0 = 82/6$, and $E_0 = 17$ for K_1; T $E_0 = 44/3$, $E_0 = 107/6$, and $E_0 = 21$ for K_2; and $E_0 = 56/3$, $E_0 = 131/6$, and $E_0 = 25$ for K_3. All other features are the same as for Fig. 9.

1. Characteristic times

A simple approach is sufficient to provide reliable estimates of the characteristic times for the energy decrease of an initially sliding dimer. The CM equation of motion, if we neglect the thermal noise, is

$$\ddot{x} = -\sin x - \gamma \dot{x}. \tag{16}$$

Let τ be the characteristic time for the CM to cover a spatial period of the periodic potential. Since the dissipation is small, we know $\tau \ll 1/\gamma$, as shown by the fact that, in the plots of the variances as functions of time, the quick oscillations are not resolved. We can therefore take a time average of the previous equation, setting $\langle\langle f(t)\rangle\rangle \equiv (1/\tau)\int_t^{t+\tau} f(u)\,\mathrm{d}u$, to get

$$\langle\langle \ddot{x}\rangle\rangle = -\gamma \langle\langle \dot{x}\rangle\rangle. \tag{17}$$

The initial value is $\langle\langle \dot{x}\rangle\rangle(0) = V_M$ from the very definition of the CM initial velocity V_M. At a time $t \gg \tau$, the time-averaged velocity is $\langle\langle \dot{x}\rangle\rangle(t) = V_M e^{-\gamma t}$. If we take into account the contribution of the underlying potential, at time t the energy of the CM is

$$\langle\langle E_x - 2\rangle\rangle(t) = \langle\langle \dot{x}\rangle\rangle^2(t) + \langle\langle 2(1-\cos x)\rangle\rangle \approx (E_0 - 2)e^{-2\gamma t}, \tag{18}$$

where the last expression results from $V_M = E_0^{1/2}(1 - 1/E_0)$, already stated in Sec. II. Roughly speaking, the initial energy is corrected by the mean energy 2 of the underlying potential. We also note that $\langle\langle E_x - 2\rangle\rangle(t) \to 0$ when $t \to \infty$. Physically, this means that the dimer leaves the sliding regime. The result of Eq. (18) s a good approximation as long as the dimer is sliding. In this case the dimer reaches a given energy E_C in a typical time

$$T_C \approx -\frac{1}{2\gamma} \ln\left(\frac{E_C - 2}{E_0 - 2}\right). \tag{19}$$

From this general formula, we may define the trapping time T_W, when the dimer becomes trapped in a potential well, if we take $E_C = 4$, so that

$$T_W \approx -\frac{1}{2\gamma} \ln\left(\frac{2}{E_0 - 2}\right). \tag{20}$$

When the initial energy is higher than the upper parametric instability $E_I^>$, which for a given stiffness K is seen to be $E_I^> = 8K$ from Eq. (12), the RM will undergo a parametric instability at a time T_I such that $E_C \approx E_I^>$, so that

$$T_I \approx -\frac{1}{2\gamma} \ln\left(\frac{8K - 2}{E_0 - 2}\right). \tag{21}$$

These two characteristic times are indicated in the variance plots displayed in Sec. III B 2 and are seen to provide good estimates.

2. Diffusion of sliding system without jumping

We display in Fig. 8 three sets of initial conditions such that the corresponding systems are not found in a jump configuration when their energy decreases due to dissipation. We will first comment the variances displayed in Fig. 9, which correspond to the systems of highest stiffness and highest initial energies that are indicated in the leftmost map of Fig. 8.

Let us consider the systems with initial representative points below the lowest instability line, which are those of lowest energies (the three yellow crosses) and those of stiffness K_3 and medium energy (the orange disk of stiffness K_3). When time goes on, their energy decreases and they stay parametrically stable. In all cases, as long as the energy is greater than 4, the variance for the CM is that of a free particle, and the variance for the RM is that of a free oscillator. When the energy of system becomes smaller than 4, these variances evolve respectively towards those of a particle and of an oscillator trapped in an anharmonic potential.

In contrast, the three systems of highest energy in Fig. 8 (left map, red squares) are initially above the instability band and cross it entirely when their energy decreases because of dissipation. Obviously, the RM variance $\sigma^2(y)$ deviates very strongly from that of a trapped oscillator as soon as the system enters the area of parametric instability. The variance $\sigma^2(y)$ reaches a maximum then slowly decreases. When the system is initially at the edge of the border of instability domain (red square, stiffness K_3), the parametric forcing induces large beats, which result in a thickening of the representative curve for $\sigma^2(y)$ observed in the corresponding plot in Fig. 9. Note that the maximum variance is roughly the same for the three systems of largest energy, but that the characteristic time T_I required to reach this maximum decreases with the stiffness. Then the systems continue to lose energy so that the variances decrease and eventually reach the thermodynamic equilibrium

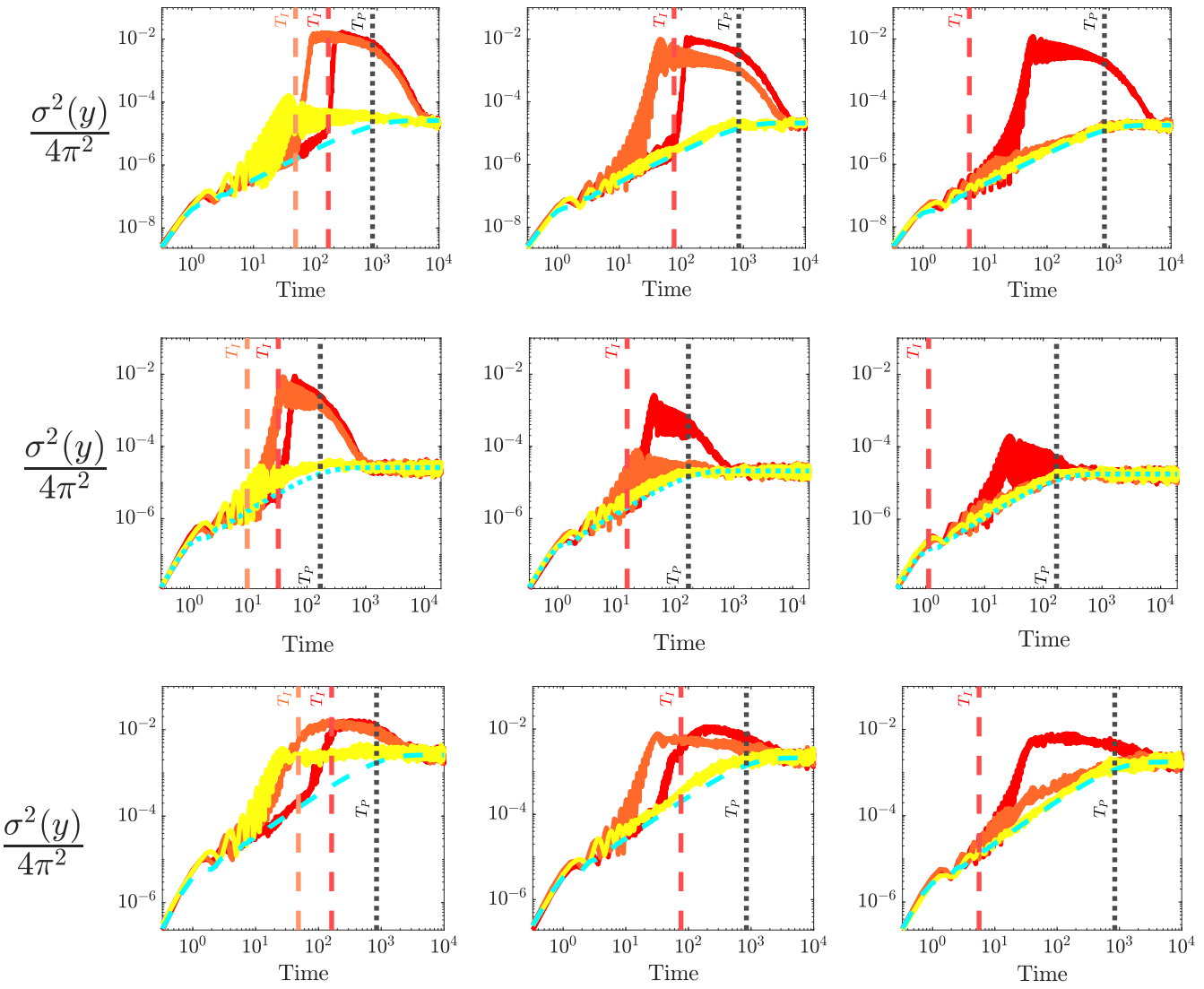

FIG. 11. Plots of the variances $\sigma^2(y)$ as a function of time, in logarithmic scales. The initial conditions are displayed in the rightmost map of Fig. 8. The stiffnesses are $K_1 = 1.1874$, $K_2 = 1.5831$, and $K_3 = 1.9789$, from left to right. The initial energies are $E_0 = 10$ (yellow, light gray, solid lines), $E_0 = 15$ (orange, medium gray, solid lines), and $E_0 = 20$ (red, dark gray, solid lines). For the top plots, the temperature is $\Theta = 7.0 \times 10^{-3}$, and the dissipation is $\gamma = 1.3 \times 10^{-3}$. For the center plots, the temperature is $\Theta = 7.0 \times 10^{-3}$, and the dissipation is $\gamma = 6.5 \times 10^{-3}$. For the bottom plots, the temperature is $\Theta = 7.0 \times 10^{-1}$, and the dissipation is $\gamma = 1.3 \times 10^{-3}$.

value $\Theta/2(2K + 1)$ when their energy is close to the thermal energy Θ.

Let us remark that the behavior of $\sigma^2(x)$ is only a weak echo of that of $\sigma^2(y)$. The variances of the CM for the four systems that evolve in a parametrically stable area (orange disk of stiffness K_3 and the three yellow crosses in the leftmost map of Fig. 8) are those of a free particle at small time and evolve toward those of a particle trapped in an anharmonic potential as soon as their energies reach 4. The variances of the highest energy systems (red squares in the leftmost map of Fig. 8) keep track of energy exchanges with the RM. As soon as the system enters its instability domain, its variance shifts to slightly higher value than that of a free particle.

Let us consider the systems of stiffness K_1 and highest energies (orange disk and red square). Both entirely cross the instability domain. The maximum reached by $\sigma^2(y)$ is the same for both systems, which suggests that the distance [in the parameters plane (K, E_0)] traveled by the representative point of the system in the instability band determines the maximum value of the RM variance. It is noticeable that the orange curve, which describes the variance of a system with lower initial energy than the red curve, exhibits the growth due to parametric instability much earlier than the red curve, in agreement with the estimated characteristic time (21). This is exactly the inverse of the temporal evolution for the variance of a trapped dimer, as we saw in Sec. III A. Indeed, for a trapped dimer, the growth of variance due to the anharmonic character of the trapping potential is made earlier as the initial energy is larger.

When the initial energy of the system is in the middle of the instability domain (orange disk with stiffness K_2), the influence of the parametric resonance on $\sigma^2(y)$ is seen from the very beginning of the motion. The duration of the parametric forcing being much less than for the system with the same

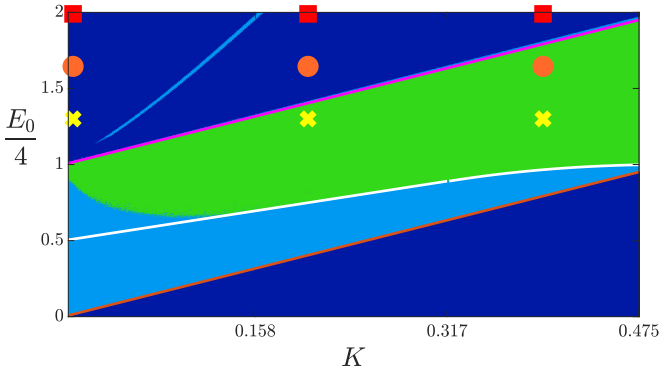

FIG. 12. Representative points for the initial energy E_0 and the stiffness K in the parameter space for the simulations described in Sec. III C. The dark blue (dark gray) areas represent a parametrically stable RM. The light blue (light gray) areas represent a parametrically unstable RM. The green (medium gray) area represents jumping motions of the system. The corresponding variances are plotted in Fig. 13, and the relevant numerical values of the stiffness K and the initial energy E_0 are given in the captions.

stiffness and higher initial energy (red square), the maximum in the variance is also smaller, as shown by the orange and red variance plots for stiffness K_2 in Fig. 9.

In order to confirm this analysis we display in Fig. 10 the variances $\sigma^2(y)$ for the set of initial conditions indicated by the representative points in the center map of Fig. 8. In contrast with the set displayed in the leftmost and rightmost maps, the colors do not indicate an equal initial energy but an equal distance to the instability curve, for a given stiffness.

In contrast with the plots of $\sigma^2(y)$ displayed in Fig. 9, and despite the fact that from left to right the stiffnesses and the initial energies are 50% higher, all sets of variance plots in Fig. 10 are roughly the same. The variations of $\sigma^2(y)$ as a function of time are very similar, with of course a long time limit at thermodynamic equilibrium that depends on the dimer stiffness and reads $\Theta/2(2K+1)$. The three yellow systems, which are initially parametrically stable, do not show any increase in their variances. The three red systems, which are initially above the instability band and cross it fully, evidence the largest increase, in their variance but this increase occurs later than for the three orange systems originally in the middle of the instability band. It can be noted, however, that the maximum variance weakly decreases with the stiffness K, and that the quick oscillations in the variance are of greater amplitude when K increases.

More precisely, in order to discuss the influence of the stiffness K on the RM variance, let us consider the systems with initial representative point given by the rightmost map in Fig. 8. The initial configurations of these systems are similar to those of the leftmost map except for lower stiffnesses. The relevant RM variances $\sigma^2(y)$ as a function of time are plotted in Fig. 11 for two dissipations γ and two temperatures Θ. We have seen in the above discussion that the maximum of the variance depends on the extent of the instability domain crossed by the representative point of the system as its energy decreases. This extent is the same for the highest initial energies (red squares), being equal to the width of the instability band. The corresponding variances (top plots of Fig. 11) evidence almost no variation with the stiffness of the maximum variance. However, if we consider the three center plots of Fig. 11, which are obtained with a five times greater dissipation, we see that an increase of the stiffness by a factor 1.65 induces a decrease of the maximum of the variance by two orders of magnitude.

Let us now consider the evolution of variance curves as a function of time when we increase the temperature Θ. To this aim we may compare the top and bottom plots of Fig. 11 since the only difference between the relevant systems is a temperature 100 times greater for the bottom plots. Obviously, the initial ballistic behavior and the asymptotic long time value of the variance are proportional to Θ. But the transient increase of the variance is such that its maximum value of $\sigma^2(y)$ is independent of the temperature, as we observed for the trapped configurations. This again suggests that the variance, although of thermal origin, has a temporal variation driven by two completely independent mechanisms, the thermal bath and the parametric resonance.

C. Diffusion when the dimer crosses the jump area

In this section we discuss the last qualitatively different configurations, that is, those that correspond to systems that can enter a zone of jumps when their energy decreases. The representative points of these configurations are shown in the map of Fig. 12. Every dimer has an initial energy greater than 4, and its stiffness is low enough for a jump regime to take place when the parametric resonance conditions are met. Nevertheless, the representative points have been chosen to display significant differences between the initial conditions, since three systems are in the jumping unstable zone from the beginning of their motion while the others are initially in a parametrically stable area.

The corresponding plots of the variances $\sigma^2(x)$ and $\sigma^2(y)$ as a function of time are given in Fig. 13 and should be compared to the variances displayed in Fig. 9. The most important difference with systems that do not undergo jumping is that the value of the maximum variance does not depend on the distance anymore [in the parameters plane (K, E_0)] traveled by the representative point of the system in the instability band. The variances $\sigma^2(y)$ of the systems with stiffness K_3 all exhibit the same maximum value. Of course, the start of variance growth occurs the sooner the system is closer to the instability area, but the maxima are roughly the same.

Another striking feature of the variance plots is that they do not reach the thermodynamic limit $\Theta/2(2K+1)$ for the variances $\sigma^2(y)$, except for the highest stiffness K_3. When the stiffness decreases (stiffnesses K_2 and K_1), the maximum of the variance remains the same, but now the particles can be eventually trapped in potential wells more than one spatial period apart. The variance $\sigma^2(y)$ for these metastable configurations is consistently higher than what should be expected for particles in adjacent wells.

This is confirmed if we plot the mean energy of the dimer, statistically averaged on 150 simulations, as a function of time as done in Fig. 14. The thermodynamic limit is $\Theta/2$, but for the lowest stiffnesses (K_2 and K_1) the system is in a metastable state of (slightly) higher energy. Of course, a possible issue could be a too short simulation time, but we think that the long

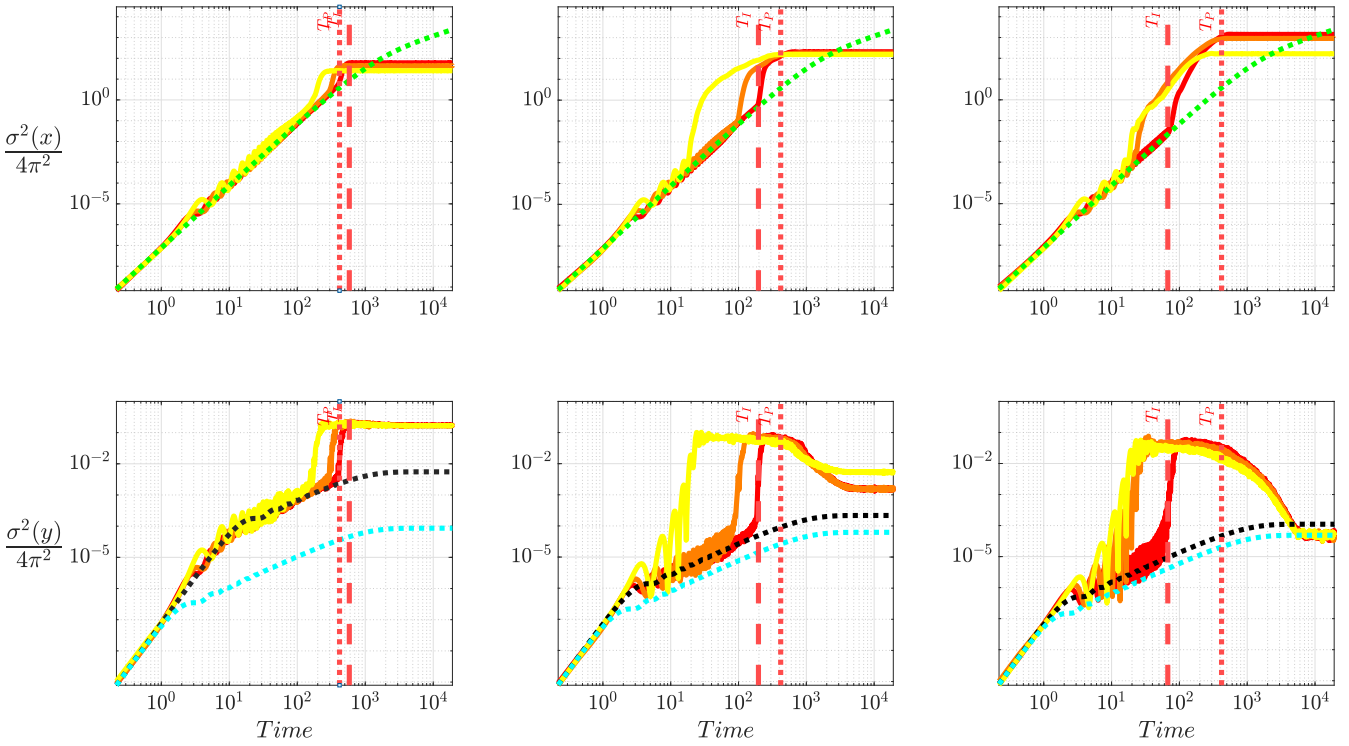

FIG. 13. Plots of the variances $\sigma^2(x)$ (top plots) and $\sigma^2(y)$ (bottom plots) as a function of time, in logarithmic scales, for the initial conditions displayed in Fig. 12, for $\Theta = 7.0 \times 10^{-3}$ and $\gamma = 1.3 \times 10^{-3}$. The stiffnesses are $K_1 = 0.0079$, $K_2 = 0.1979$, and $K_3 = 0.3958$, in increasing order from left to right. The initial energies are $E_0 = 5.20$ (yellow, light gray, solid line), $E_0 = 6.58$ (orange, medium gray, solid line), and $E_0 = 8.00$ (red, dark gray, solid line). The green dashed lines correspond to the diffusion of a single free particle, the cyan dashed lines to the diffusion of a single particle in an harmonic well of frequency $\sqrt{2K+1}$. The times T_I of Eq. (21) are indicated by dashed lines of the same color as the relevant plot, the time T_P by a black dotted line.

time stationary behaviors observed in the plots of the CM and RM trajectories displayed in Fig. 15 and Fig. 16 evidence that we have indeed reached a (quasi) equilibrium state.

We can get further insight in the dynamics of the dimer if we plot some trajectories as a function of time for a given temperature and a given dissipation. This is done in Fig. 15

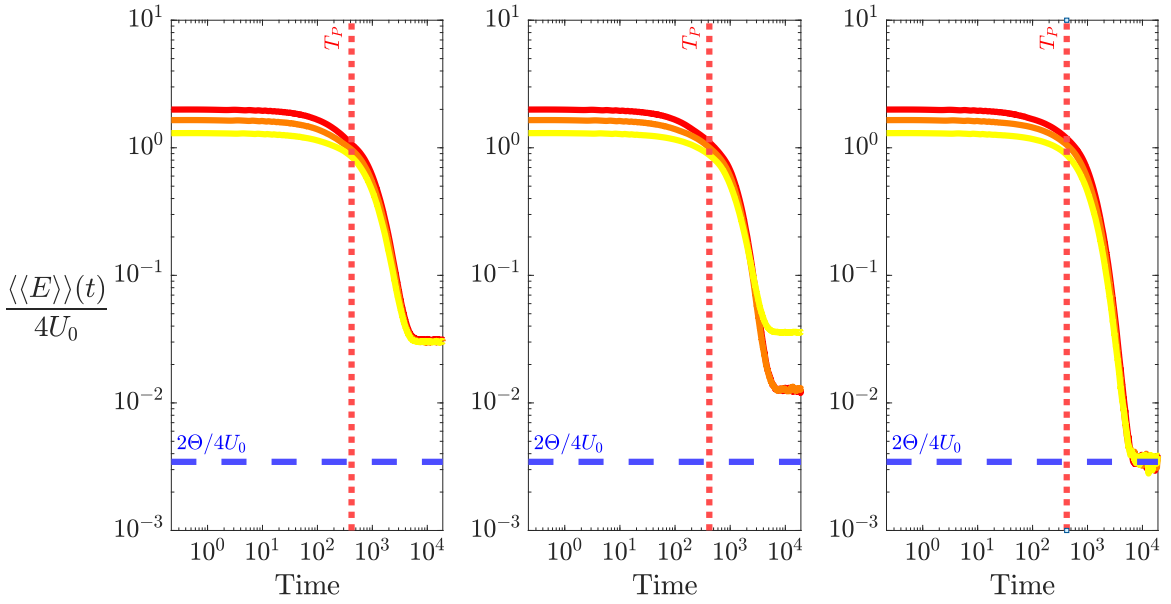

FIG. 14. Mean energy of the dimer as a function of time, in logarithmic scales, for $\Theta = 7.0 \times 10^{-3}$ and $\gamma = 1.3 \times 10^{-3}$. The stiffnesses are $K_1 = 0.0079$, $K_2 = 0.1979$, and $K_3 = 0.3958$, in increasing order from left to right. The initial energies are $E_0 = 5.20$ (yellow, light gray, solid line), $E_0 = 6.58$ (orange, medium gray, solid line), and $E_0 = 8.00$ (red, dark gray, solid line). The blue dashed line correspond to the thermodynamic equilibrium.

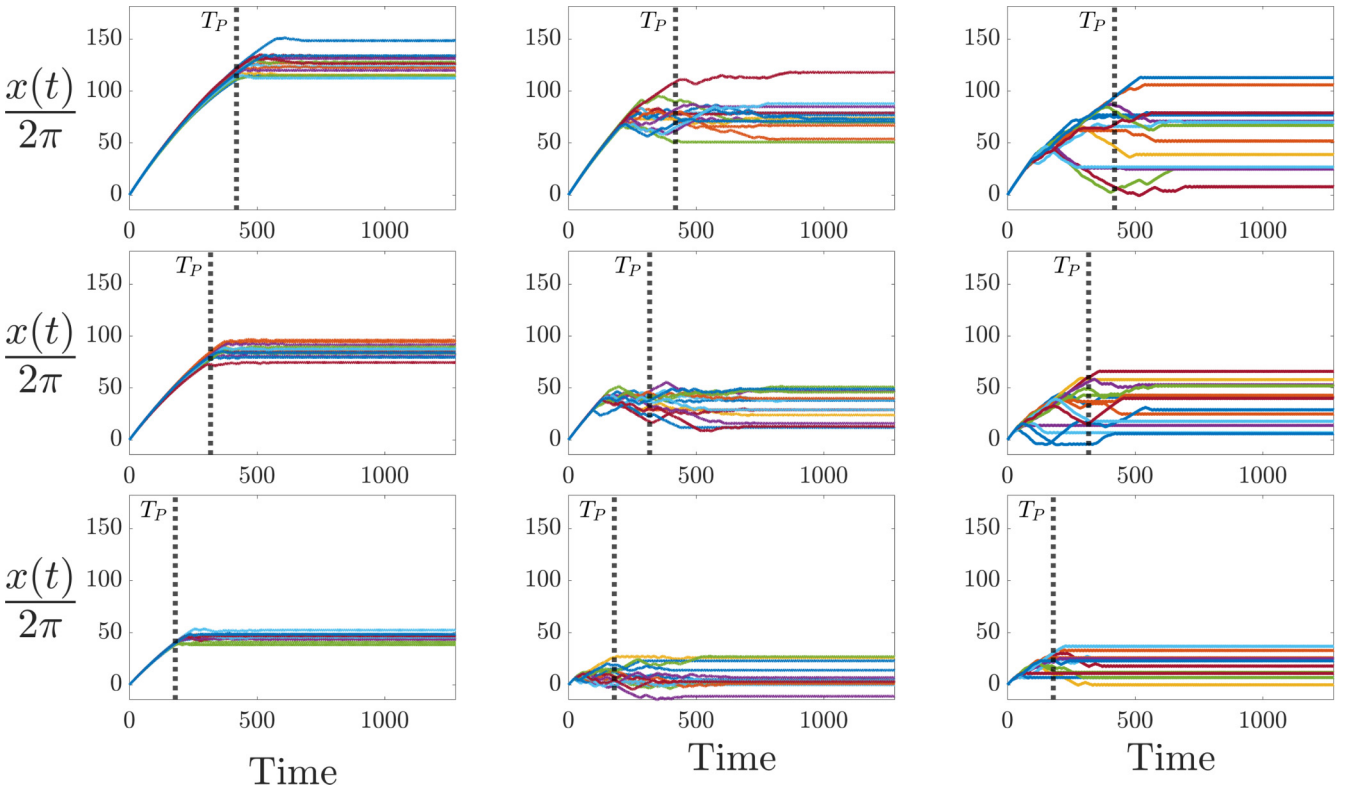

FIG. 15. Some CM trajectories as a function of time (linear scales) for the initial conditions of Fig. 12. For each column the stiffnesses are $K_1 = 0.0079$, $K_2 = 0.1979$, and $K_3 = 0.3958$, in increasing order from left to right. For each line the initial energies are $E_0 = 5.20$, $E_0 = 6.58$, and $E_0 = 8.00$, in decreasing order from top to bottom. The temperature is $\Theta = 7.0 \times 10^{-3}$, and the dissipation is $\gamma = 1.3 \times 10^{-3}$. The colors are arbitrary.

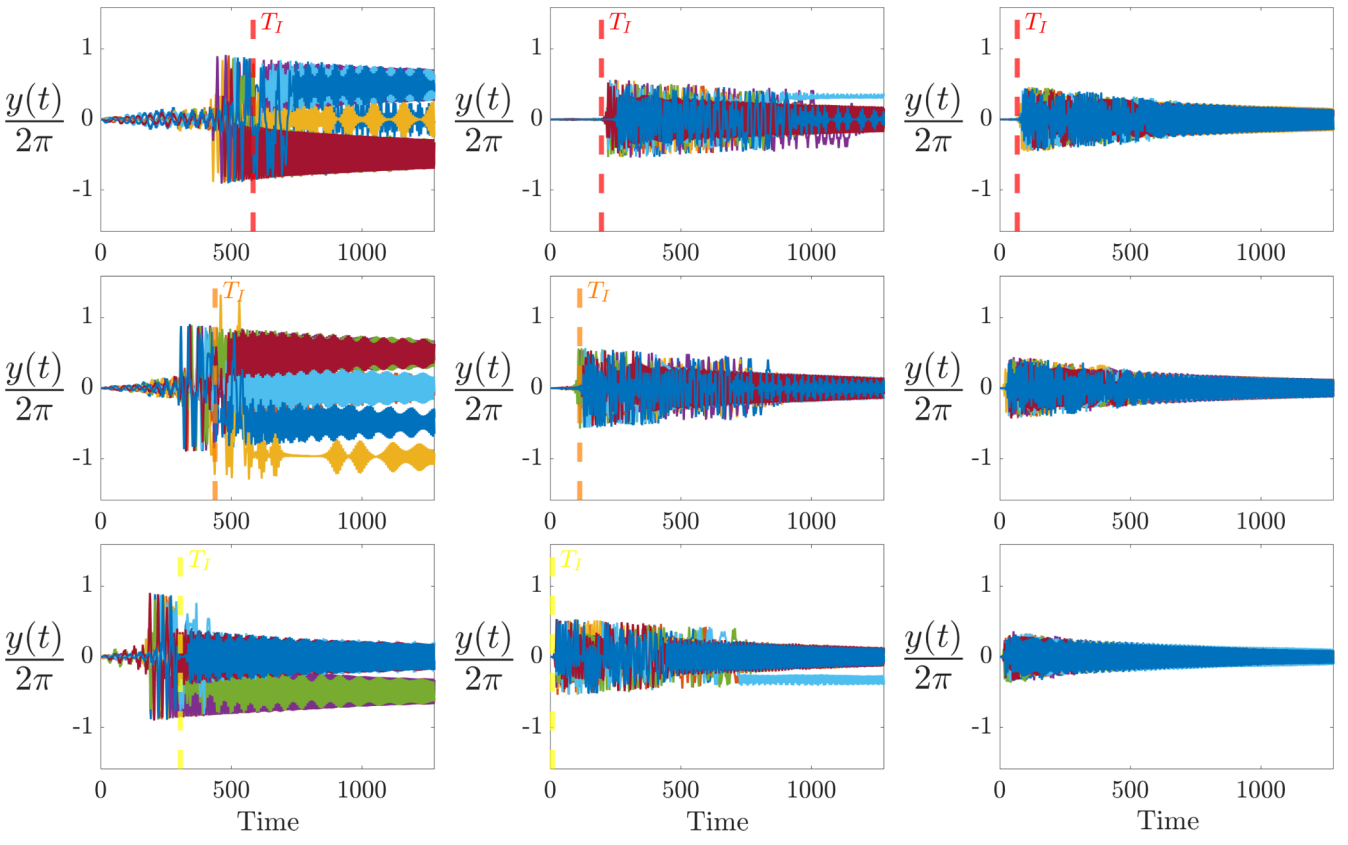

FIG. 16. Same as Fig. 15, but for the RM trajectories as a function of time (linear scales).

for the CM trajectories. We see that at larger stiffnesses, the final position of the CM is widely dispersed among potential wells. This is consistent with the increase in the variances $\sigma^2(x)$ plotted in Fig. 13 that are seen at high stiffnesses. If we consider trajectories of the RM, as shown in Fig. 16, they exhibit a completely opposite behavior. In this latter case, a large dispersion of the RM trajectories is observed at small stiffnesses. This is consistent with the large long time value of the variance $\sigma^2(y)$ displayed in Fig. 13 and with the metastable thermodynamic state evidenced by the statistically averaged energy of the dimer in Fig. 14 (note that since all potential wells are equivalent, this energy do not depends on the equilibrium position of the CM).

These behaviors are fully consistent with the detailed analysis of the jumping regime undertaken in Ref. [33]. We have shown that two distinct jumping regimes happen. At large stiffness, the dimer is not deformed but the CM trajectory is almost random, so that if we add dissipation the eventual position of the CM is widely dispersed. At small stiffness, in contrast, the dimer is very deformed, and the jumping regime corresponds to configurations in which the dimer particles are not in adjacent potential wells.

IV. CONCLUSION

In this study we have investigated the behaviors of the variances of the translation mode and relative displacement mode describing the dynamics of a dimer diffusing over a commensurate underlying periodic potential. A particular focus has been put on the influence of the parametric resonance of the relative motion induced by the center of mass motion on the diffusion, and on its feedback on the center of mass motion.

Because of the dissipation, the system loses its energy and follows a trajectory of constant stiffness but decreasing energy in the parameters plane (initial energy E_0, stiffness K), down to the thermodynamic equilibrium. We have shown that the evolution of variances is closely related to this trajectory. According to the initial values (E_0, K) the dimer is either parametrically stable at all time, or parametrically unstable during part of its movement, when the relevant representative point in the parameter plane crosses its instability domain.

When the dimer is initially unstable and out of a jumping zone, the parametric resonance of the RM induces a strong and transient increase of its variance. The amplitude of the increase depends on the extent of the instability domain crossed, and the larger the domain crossed, the greater the variance increase. This transient decreases with the damping coefficient. When the system leaves its parametric instability zone, but the energy remains high, the CM and RM modes diffuse as a particle in an anharmonic potential well. The resulting variances exhibit an unusual enhancement with respect to diffusion in a quadratic potential, which depends on the energy of the system when it leaves the instability area and is the greater the higher this energy. Eventually, at very long time, all initial energy above the thermal energy is lost, and both modes diffuse as effective particles in a quadratic potential.

The situation differs when the system crosses the entire area of instability including a jumping zone. In this case, the evolution with time of variances differs considerably from the previous one. New factors come into play, in particular dimer deformations and potential elastic energy stored in these deformations, in such a way that the system may stay in a metastable configuration.

Such effects of the parametric resonance on the diffusion of modes may be also observed on larger systems which have many modes of vibration [38]. A forthcoming paper will discuss our observations for a trimer in which two modes of vibration may be excited by the translation mode and for a large chain in which the small frequency distance between modes allows new specific behaviors.

Last, let us note that some attempts of theoretical analysis of these behaviors have been made. The theoretical analysis of the diffusion of a particle whose dynamics obeys a linear Mathieu equation in the presence of a Gaussian thermal noise was made a few years ago [39–42]. It shows that the high-time stationary value of the mean square displacement of the particle position increases as the system approaches its zone of instability and diverges on the instability boundary. However, this model is valid only for a linear Mathieu equation with a forcing amplitude and frequency considered constant in time. Therefore the obtained variance is stationary. Our case of autoparametric resonance is much more complex because the equations describing the coupling between the modes are nonlinear and because their characteristic parameters change with time.

[1] H. Risken, *The Fokker-Planck Equation* (Springer, Berlin, 1989).

[2] R. Festa and E. G. d'Agliano, Diffusion coefficient for a Brownian particle in a periodic field of force, Physica A **90**, 229 (1978).

[3] D. Weaver, Effective diffusion coefficient of a Brownian particle in a periodic potential, Physica A **98**, 359 (1979).

[4] L. Gunther, M. Revzen, and A. Ron, Mobility in a periodic potential: A simple derivation, Physica A **95**, 367 (1979).

[5] F. Jülicher, A. Ajdari, and J. Prost, Modeling molecular motors, Rev. Mod. Phys. **69**, 1269 (1997).

[6] P. Hänggi and F. Marchesoni, Artificial Brownian motors: Controlling transport on the nanoscale, Rev. Mod. Phys. **81**, 387 (2009).

[7] P. Brüesch, L. Pietronero, S. Strässler, and H. R. Zeller, Brownian motion in a polarizable lattice: Application to superionic conductors, Phys. Rev. B **15**, 4631 (1977).

[8] P. Burada, G. Schmid, P. Talkner, P. Hänggi, D. Reguera, and J. Rubi, Entropic particle transport in periodic channels, Biosystems **93**, 16 (2008).

[9] M. Borromeo and F. Marchesoni, Resonant transport in pulsated devices: Mobility oscillations and diffusion peaks, Phys. Rev. E **78**, 051125 (2008).

[10] S. Bleil, P. Reimann, and C. Bechinger, Directing Brownian motion by oscillating barriers, Phys. Rev. E **75**, 031117 (2007).

[11] P. Fulde, L. Pietronero, W. Schneider, and S. Strässler, Problem of Brownian motion in periodic potential, Phys. Rev. Lett. **35**, 1776 (1975).

[12] W. Dieterich, I. Peschel, and W. R. Schneider, Diffusion in periodic potentials, Z. Phys. B **27**, 177 (1977).
[13] G. Costantini and F. Marchesoni, Threshold diffusion in a tilted washboard potential, Europhys. Lett. **48**, 491 (1999).
[14] T. E. Harris, Diffusion with "collisions" between particles, J. Appl. Probab. **2**, 323 (1965).
[15] D. G. Levitt, Dynamics of a single file pore: Non-Fickian behavior, Phys. Rev. A **8**, 3050 (1973).
[16] M. Kollmann, Single-file diffusion of atomic and colloidal systems: Asymptotic laws, Phys. Rev. Lett. **90**, 180602 (2003).
[17] A. Taloni and M. A. Lomholt, Langevin formulation for single-file diffusion, Phys. Rev. E **78**, 051116 (2008).
[18] J.-B. Delfau, C. Coste, C. Even, and M. Saint Jean, Single-file diffusion of interacting particles in a finite-sized channel, Phys. Rev. E **82**, 031201 (2010).
[19] J.-B. Delfau, C. Coste, and M. Saint Jean, Single file diffusion of particles with long-ranged interactions: Damping and finite size effects, Phys. Rev. E **84**, 011101 (2011).
[20] G. Coupier, M. Saint Jean, and C. Guthmann, Single file diffusion enhancement in a fluctuating modulated quasi-1D channel, Europhys. Lett. **77**, 60001 (2007).
[21] T. Dessup, C. Coste, and M. Saint Jean, Enhancement of Brownian motion for a chain of particles in a periodic potential, Phys. Rev. E **97**, 022103 (2018).
[22] C. Cattuto and F. Marchesoni, Unlocking of an elastic string from a periodic substrate, Phys. Rev. Lett. **79**, 5070 (1997).
[23] O. M. Braun, R. Ferrando, and G. E. Tommei, Stimulated diffusion of an adsorbed dimer, Phys. Rev. E **68**, 051101 (2003).
[24] E. Heinsalu, M. Patriarca, and F. Marchesoni, Dimer diffusion in a washboard potential, Phys. Rev. E **77**, 021129 (2008).
[25] C. Fusco, A. Fasolino, and T. Janssen, Nonlinear dynamics of dimers on periodic substrates, Eur. Phys. J. B **31**, 95 (2003).
[26] S. Y. Krylov, Surface gliding of large low-dimensional clusters, Phys. Rev. Lett. **83**, 4602 (1999).
[27] O. Braun, Adiabatic motion of an atomic chain in periodic potential, Surf. Sci. **230**, 262 (1990).
[28] O. M. Braun, Role of entropy barriers for diffusion in the periodic potential, Phys. Rev. E **63**, 011102 (2000).
[29] C. Fusco and A. Fasolino, Microscopic mechanisms of thermal and driven diffusion of non rigid molecules on surfaces, Thin Solid Films **428**, 34 (2003).
[30] M. Patriarca, P. Szelestey, and E. Heinsalu, Brownian model of dissociated dislocations, Acta Phys. Pol. B **36**, 1745 (2005).
[31] D. S. Sholl and K. A. Fichthorn, Concerted diffusion of molecular clusters in a molecular sieve, Phys. Rev. Lett. **79**, 3569 (1997).
[32] J. Maddi, C. Coste, and M. Saint Jean, Parametric resonance in a conservative system of coupled nonlinear oscillators, Phys. Rev. E **105**, 054208 (2022).
[33] J. Maddi, C. Coste, and M. Saint Jean, Motions of a dimer on a periodic potential, Phys. Rev. E **106**, 064201 (2022).
[34] N. W. McLachlan, *Theory and Applications of Mathieu Functions* (Clarendon Press, Oxford, 1951).
[35] L. Brillouin, *Wave Propagation in Periodic Structures* (Dover, 1953).
[36] D. T. Gillespie, Exact numerical simulation of the Ornstein-Uhlenbeck process and its integral, Phys. Rev. E **54**, 2084 (1996).
[37] D. T. Gillespie, The mathematics of Brownian motion and Johnson noise, Am. J. Phys. **64**, 225 (1996).
[38] J. Maddi, Dynamique déterministe et stochastique de systèmes élastiques unidimensionnels soumis à un potentiel périodique: Effets de la résonance autoparamétrique., Ph.D. thesis, Université Paris Cité, 2023.
[39] A. A. Batista and R. S. N. Moreira, Signal-to-noise ratio in parametrically driven oscillators, Phys. Rev. E **84**, 061121 (2011).
[40] A. A. Batista, Squeezing of thermal noise in a parametrically driven resonator, J. Phys.: Conf. Ser. **285**, 012041 (2011).
[41] A. A. Batista, Cooling, heating, and thermal noise squeezing in a parametrically driven resonator, J. Stat. Mech. (2011) P02007.
[42] C. Zerbe, P. Jung, and P. Hänggi, Brownian parametric oscillators, Phys. Rev. E **49**, 3626 (1994).